Acta Mech 226, 1133–1151 (2015)
DOI 10.1007/s00707-014-1237-7

H. A. F. A. Santos

A novel updated Lagrangian complementary energy-based formulation for the elastica problem: force-based finite element model

Received: 19 September 2013 / Revised: 6 August 2014 / Published online: 24 September 2014

Abstract This paper addresses the development of a novel updated Lagrangian variational formulation and its associated finite element model for the geometrically nonlinear quasi-static analysis of cantilever beams. The formulation is based on an incremental complementary energy principle. The proposed finite element model only contains nodal bending moments as degrees of freedom. The model is used for the analysis of problems modeled by the so-called elastica theory. Numerical solutions satisfying all equilibrium equations in a strong sense can be obtained for arbitrarily large displacements and rotations. A Newton–Raphson method is adopted to trace the post-buckling response. Numerical results are presented and compared with those produced by the standard total Lagrangian two-node displacement-based finite element model.

1 Introduction

The study of large deflections of thin beams has received a growing interest in many engineering and science problems. Examples of these problems include: framed structures [27,34,35], compliant mechanisms [8,43], biological (DNA molecules) and nanoscale structures [29,44,46], and computer vision [10,24,30].

The simplest geometrically nonlinear bending theory of thin beams is the so-called *elastica theory* (sometimes also called Euler–Bernoulli elastica theory) [17,28]. The formulation and solution of the elastica problem date back to James Bernoulli, Daniel Bernoulli and Euler, and have a long and rich history [20,45]. In the framework of this theory, a beam is thought of as an inextensible line of particles, which resists bending according to a law given by a linear constitutive relation. Further, no restrictions on the magnitude of displacements or angles of rotation are considered. Several variants to the elastica theory have been proposed in the literature, in particular, theories including dynamical effects, extensibility [22], shear deformation [2,23], plasticity, and follower loads, see e.g., also [1] and the references therein.

Different approaches have been proposed for the analysis of elastic thin beam problems: (i) the elliptic integral approach, first proposed in [6,36], which gives closed-form solutions for simple loading cases and boundary conditions, see e.g., [23,31] for more details on this approach, (ii) the numerical integration approach with iterative shooting techniques, e.g., [11,26,32], and (iii) the incremental finite element method with Newton–Raphson iteration techniques [18,19,42]. Of these approaches, the finite element method is indeed the most popular approach, mainly due to its versatility to the analysis of problems with complex topologies and geometries. As a result, numerous geometrically nonlinear finite thin beam elements have been developed over the past few decades. Fairly recently, B-spline-based isogeometric methods have also been proposed in the framework of elastic thin beam problems [16,25].

H. A. F. A. Santos (✉)
Instituto Superior de Educação e Ciências, Alameda das Linhas de Torres 179, 1750-142
Lisboa, Portugal
E-mail: hugofreixialsantos@gmail.com

The numerical implementation of structural mechanics problems by the finite element method has been performed mostly by resorting to displacement-based variational formulations, such as the well-known Principle of Stationary Total Potential Energy (PSTPE), or the Principle of Virtual Work [47]. A shortcoming of these formulations is that their resulting finite element models lead, in general, to stress discontinuities across interelement boundaries. As a result, and since for many engineering purposes, the stress distribution is, very often, the paramount information needed, applications of these models usually involve an averaging procedure to obtain piecewise-smooth stress distributions for design calculations.

Models that avoid the need for these averaging procedures are the so-called equilibrium models, introduced in [13,14] for small deformation problems. These models are usually formulated on the basis of the so-called Principle of Stationary Total Complementary Energy (PSTCE), or the Principle of Complementary Virtual Work [47], and are capable of producing statically admissible solutions, i.e., solutions satisfying in strong form the equilibrium differential equations, as well as the equilibrium boundary conditions.

When used in conjunction, and in the framework of small elastic deformation problems, displacement and equilibrium models may be used to determine upper bounds of the error of an approximate solution with respect to the theoretically exact solution [14,15]. This is essential for a reliable application of the models, as it allows to assess the accuracy of the finite element approximations.

However, although displacement-based models have been developed for both small and large deformation problems, equilibrium models have been developed, almost exclusively, for small deformation problems.

We believe this stems from the fact that, although for small deformation problems both the PSTPE and the PSTCE are only expressed in terms of displacement-like and stress-like variables, respectively, when large deformations are assumed to be dealt with, even though the PSTPE can still be expressed only in terms of displacement variables, the PSTCE cannot, in general, be expressed only in terms of stress-like variables, due to the nonlinear coupling between stresses and displacements in the equilibrium equations of large deformation problems. This may engender technical complications, as it requires the use of mixed approximation schemes in the framework of the equilibrium models.

Equilibrium models are particularly attractive for geometrically nonlinear one-dimensional models, such as beams and cables, due to their ability to provide exact equilibrium satisfaction in a more straightforward way than in other types of structural elements, such as plates or shells.

Nevertheless, only a few studies have been addressed to the development of equilibrium models from which statically admissible solutions can be obtained for beam problems. The original ideas of geometrically nonlinear mixed finite beam elements were proposed in [3,9]. Almost one decade later, an equilibrium model for geometrically nonlinear Euler–Bernoulli beams with moderately large deflections was introduced in [33]. A variationally consistent finite element model for the geometrically nonlinear first-order analysis of Euler–Bernoulli framed structures has recently been proposed in [38]. This model relies on a pure complementary energy principle and only involves force-like variables as fundamental unknowns, being therefore a true force-based finite element model. However, all these models are only valid for moderately large deflections.

Equilibrium models for the analysis of framed structures with arbitrarily large displacements and rotations were proposed in [37,39,41]. However, these models rely on two-field complementary energy principles, involving not only stress resultants, but also displacement variables as fundamental unknowns. An exception is the recently introduced force-based equilibrium finite element model for nonlinear elastic cables with arbitrarily large strains [40], which was derived from a complementary energy principle only involving force-like quantities.

All of the aforementioned finite element models are based on total Lagrangian approaches, i.e., approaches in which all static and kinematic variables are referred to the initial configuration at time 0 [12]. This is the reason why such models need, in general, to be mixed models involving both force-like and displacement-like variables. A possible strategy to build force-based equilibrium models for geometrically nonlinear one-dimensional beam problems is to resort to updated Lagrangian schemes [4,5], in which all variables are referred to the configuration at time t. In fact, from a numerical point of view, geometrically nonlinear problems need, in general, to be addressed by resorting to series of linearized problems solved in an incremental/iterative fashion. Hence, incremental updated Lagrangian models may be well suited for the development of force-based equilibrium models, i.e., models that only involve force-like variables, for the analysis of geometrically nonlinear problems.

It is the purpose of this paper to: (i) introduce an incremental complementary energy principle only expressed in terms of incremental bending moments for the geometrically nonlinear quasi-static analysis of plane cantilever beam problems of the Euler–Bernoulli *elastica* type; (ii) derive a novel variationally consistent force-based updated Lagrangian equilibrium finite element beam formulation; (iii) develop a new

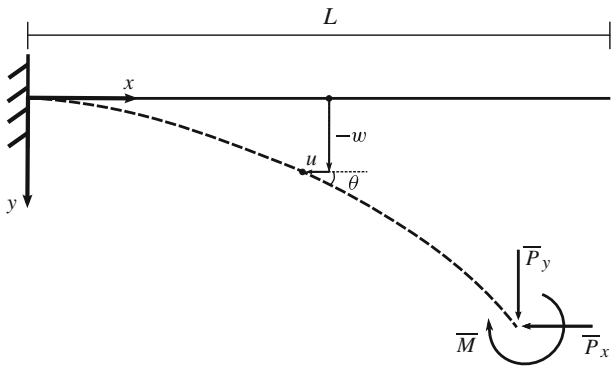

Fig. 1 Elastica problem

two-node, rotation-free, finite element for the analysis of cantilever beam problems with arbitrarily large displacements and rotations. The proposed model resembles the standard C^0-continuous Lagrange (or two-node) displacement-based model with piecewise-linear rotations.

The paper is organized as follows: The set of governing differential equations and boundary conditions is first introduced in Sect. 2, followed by the total energy principles associated with the boundary-value problem under analysis, given in Sect. 3. The incremental form of the complementary energy principle that will be used as the basis for the derivation of the finite element model is then presented in Sect. 4. The updated Lagrangian equilibrium force-based finite element model is afterward derived in Sect. 5. Some numerical tests are analyzed in Sect. 6 and, finally, some conclusions are drawn in Sect. 7.

2 Boundary-value problem

Without loss of generality, let us consider an initially straight cantilever thin beam, or elastica, of length L subjected to a pair of concentrated loads $\overline{P}_x$ and $\overline{P}_y$, and also a bending moment $\overline{M}$ applied at its tip, as illustrated in Fig. 1. Let also $x \in [0, L]$ denote a point of the elastica in its undeformed reference configuration.

The governing differential equations of the elastica in a quasi-static regime are given as follows, see e.g., [28]

$$EIM' + \overline{P}_x \sin(\theta) + \overline{P}_y \cos(\theta) = 0, \tag{1.1}$$

$$\kappa - \theta' = 0, \tag{1.2}$$

$$M - EI\kappa = 0 \tag{1.3}$$

which represent the equilibrium, kinematic, and constitutive equations, respectively, where $M = M(x)$ represents the bending moment field, $\theta = \theta(x)$ represents the rotation angle of the normal to the elastica, $\kappa = \kappa(x)$ is the curvature field, EI is the bending stiffness, assumed constant, with E the Young's modulus and I the cross-sectional moment of inertia. $(\cdot)'$ represents differentiation of $(\cdot)$ with respect to x.

The equilibrium and kinematic boundary conditions are

$$M(L) - \overline{M} = 0, \tag{2.1}$$

$$\theta(0) = 0. \tag{2.2}$$

Additionally, the horizontal and vertical displacements of the elastica, herein denoted by $u = u(x)$ and $w = w(x)$, respectively, see Fig. 1, must satisfy the following conditions:

$$1 + u' - \cos(\theta) = 0, \tag{3.1}$$

$$w' - \sin(\theta) = 0, \tag{3.2}$$

$$u(0) = w(0) = 0. \tag{3.3}$$

As is well known, the boundary-value problem defined by (1–3) may exhibit multiple solutions, very often referred to as *elastica shapes*. A number of alternative variational (or weak) formulations of the present

boundary-value problem can be developed. Variational formulations are well suited for the development of consistent numerical methods, such as the finite element method. We introduce in the following section the one-field principle of total potential energy, the two-field principle of complementary Hellinger–Reissner energy, and also a two-field principle of total complementary energy associated with the present boundary-value problem. The latter will be used as a starting point for the development of a pure incremental principle of complementary energy, which in turn will be used as the variational basis for the construction of the proposed force-based finite element model for the elastica problem.

3 Total energy principles

As is well known, each elastica shape corresponds to a stationary point of the total potential energy functional, $\Pi_p(\theta) : \mathcal{U}_\mathrm{k} \to \mathcal{R}$, defined by

$$\Pi_p(\theta) = \int_0^L \left(\frac{1}{2} EI\theta'^2 \, \mathrm{d}x + \overline{P}_x \big(\cos(\theta) - 1 \big) - \overline{P}_y \sin(\theta) \right) \mathrm{d}x - \overline{M}\theta(L) \tag{4}$$

with $\mathcal{U}_\mathrm{k}$ the kinematically admissible space defined as

$$\mathcal{U}_\mathrm{k} = \big\{ \theta \in \mathcal{H}^1 \, : \, \theta(0) = 0 \big\} \tag{5}$$

where $\mathcal{H}^1$ represents a standard Hilbert space.

It can be easily seen that, of all kinematically admissible rotation fields θ, those that satisfy the equilibrium differential equations and equilibrium boundary conditions are the ones for which the total potential energy assumes a stationary value. This result constitutes the so-called PSTPE for the elastica problem.

Departing from this variational principle, different energy principles can be formulated by means of the so-called Lagrange multiplier method [47]. Examples of this include: three-field principles of Hu–Washizu type, two-field principles of Hellinger–Reissner type, or the principle of complementary energy. Aiming at developing a force-based finite element approach for the elastica problem, we are particularly interested in the development of a complementary energy-based variational formulation of the boundary-value problem presented in the preceding section.

There are three main steps one needs to take to derive the complementary energy functional from the potential energy functional. First, the so-called Legendre transformation is needed to replace the strain energy density by its counterpart complementary form. In the present case, the Legendre transformation may be written as

$$\frac{1}{2} EI\theta'^2 = M\kappa - \frac{1}{2} \frac{M^2}{EI}. \tag{6}$$

Second, the kinematic equations (1.2) and (2.2) need to be relaxed in the framework of the total potential energy. This can be accomplished by means of the Lagrange multiplier method, which, after multiplying the total potential energy Π_p by -1, gives the following complementary Hellinger–Reissner energy, $\Pi_{HR}(M, \theta) : \mathcal{H}^0 \times \mathcal{H}^1 \to \mathcal{R}$,

$$\Pi_{HR}(M, \theta) = \int_0^L \left(\frac{1}{2} \frac{M^2}{EI} - M\theta' - \overline{P}_x \big(\cos(\theta) - 1 \big) + \overline{P}_y \sin(\theta) \right) \mathrm{d}x + \overline{M}\theta(L) - M(0)\theta(0) \tag{7}$$

with $\mathcal{H}^0$ and $\mathcal{H}^1$ the standard Sobolev spaces. Note that, in the variational setting of this principle, there are no subsidiary conditions, i.e., a pair (M, θ) need not satisfy a priori either the equilibrium or the kinematic equations.

Finally, the complementary energy functional may be derived from the complementary Hellinger–Reissner energy Π_{HR} by introducing the equilibrium equations (1.1) and (2.1), into its variational framework. This may again be accomplished using the Lagrange multiplier method. The result is the two-field functional, $\Pi_c(M, \theta) : \mathcal{U}_\mathrm{s} \to \mathcal{R}$, defined by

$$\Pi_c(M, \theta) = \int_0^L \left(\frac{1}{2} \frac{M^2}{EI} - \overline{P}_x \big(\cos(\theta) - 1 + \theta \sin(\theta) \big) + \overline{P}_y \big(\sin(\theta) - \theta \cos(\theta) \big) \right) dx \tag{8}$$

with $\mathcal{U}_{\mathrm{s}}$ the statically admissible space given by

$$\mathcal{U}_{\mathrm{s}} = \left\{(M,\theta) \in \mathcal{H}^1 \times \mathcal{H}^0 :\ EIM' + \overline{P}_x \sin(\theta) + \overline{P}_y \cos(\theta) = 0,\ M(L) - \overline{M} = 0\right\}. \tag{9}$$

As can be seen, among all statically admissible pairs (M,θ), those which render a stationary complementary energy satisfy the kinematic differential equations (1.2) and the kinematic boundary conditions (2.2), corresponding therefore to a solution of the boundary-value problem. This result will hereafter be referred to as the PSTCE for the elastica problem. To the author's best knowledge, it is the first time that the PSTCE is formulated in the framework of the elastica problem.

Note that the PSTCE plays the dual role of the PSTPE presented previously. It is also worth mentioning that, in the present case, the total complementary energy appears as a two-field functional, involving not only the bending moment field, but also the rotation field. Hence, unlike the small deformation case, a stationary point of Π_c does not represent, in general, a maximum point but rather a saddle point. In the finite element context, this may engender technical complications, as it requires the use of mixed-type numerical discretization schemes, which may suffer from numerical stability issues. In contrast, numerical formulations relying on one-field (or pure) variational approaches, such as the traditional displacement-based formulation, are unconditionally stable. Therefore, one-field variational approaches are particularly well suited for the development of reliable finite element approaches. One possible way to avoid the use of mixed (also called multi-field) variational formulations is to resort to incremental-based variational approaches. We introduce in the next section a novel incremental principle of complementary energy only involving force-like variables as fundamental unknowns. This principle will later on be used for the development of a force-based updated Lagrangian finite element model for the elastica problem.

4 Pure incremental principle of complementary energy

Let S_0 be the initial known state of the elastica, and let S_n and S_{n+1} be the states prior to and after the addition of the $(n+1)$-th increment of applied loads, respectively. The states S_n and S_{n+1} are assumed to be incrementally close to one another, which allows all the governing equations to be linearized with respect to the incremental quantities. Let $(\cdot)_n$ denote the variable in S_n and $\Delta(\cdot)$ the change in the corresponding variable from the known state S_n to the incrementally close neighbouring state S_{n+1}.

Toward the development of the pure incremental principle of complementary energy, let us first derive the incremental form of the complementary Hellinger–Reissner principle.

The complementary Hellinger–Reissner energies in states S_n and S_{n+1} are

$$\Pi_{HR_n} = \int_0^L \left(\frac{M_n^2}{2EI} - M_n\theta_n' - \overline{P}_{x_n}\left(\cos(\theta_n) - 1\right) + \overline{P}_{y_n}\sin(\theta_n)\right) dx + \overline{M}_n\theta_n(L) - M_n(0)\theta_n(0) \tag{10}$$

and

$$\begin{aligned}\Pi_{HR_{n+1}} = \int_0^L \Bigg(&\frac{(M_n+\Delta M)^2}{2EI} - (M_n+\Delta M)(\theta_n'+\Delta\theta') \\ &- (\overline{P}_{x_n}+\Delta\overline{P}_x)\left(\cos(\theta_n) - \sin(\theta_n)\Delta\theta - \frac{1}{2}\cos(\theta_n)\Delta\theta^2 - 1\right) \\ &+ (\overline{P}_{y_n}+\Delta\overline{P}_y)\left(\sin(\theta_n) + \cos(\theta_n)\Delta\theta - \frac{1}{2}\sin(\theta_n)\Delta\theta^2\right)\Bigg) dx \\ &+ \left(\overline{M}_n + \Delta\overline{M}\right)\left(\theta_n(L) + \Delta\theta(L)\right) - \left(M_n(0) + \Delta M(0)\right)\left(\theta_n(0) + \Delta\theta(0)\right)\end{aligned} \tag{11}$$

where the following relations were used in (11):

$$\cos(\theta_{n+1}) = \cos(\theta_n) - \sin(\theta_n)\Delta\theta - \frac{1}{2}\cos(\theta_n)\Delta\theta^2, \tag{12.1}$$

$$\sin(\theta_{n+1}) = \sin(\theta_n) + \cos(\theta_n)\Delta\theta - \frac{1}{2}\sin(\theta_n)\Delta\theta^2. \tag{12.2}$$

Note that these relations correspond to series expansions about θ_n in which only terms up to second-order are retained, being therefore valid for moderately large rotations.

Subtracting (10) from (11), the incremental form of the complementary Hellinger–Reissner energy comes out as

$$\begin{aligned}\Delta\Pi_{HR}(\Delta M,\Delta\theta)=\int_0^L\Bigg(&\frac{M_n\Delta M}{EI}+\frac{\Delta M^2}{2EI}-M_n\Delta\theta'-\Delta M(\theta_n'+\Delta\theta')+\left(\overline{P}_{x_n}\sin(\theta_n)+\overline{P}_{y_n}\cos(\theta_n)\right)\Delta\theta\\&-\Delta\overline{P}_x\left(\cos(\theta_n)-\sin(\theta_n)\Delta\theta-1\right)+\Delta\overline{P}_y(\sin(\theta_n)+\cos(\theta_n)\Delta\theta)\\&+\frac{1}{2}\left(\overline{P}_{x_n}+\Delta\overline{P}_x\right)\cos(\theta_n)\Delta\theta^2-\frac{1}{2}\left(\overline{P}_{y_n}+\Delta\overline{P}_y\right)\sin(\theta_n)\Delta\theta^2\Bigg)\,dx\\&+\overline{M}_n\Delta\theta(L)+\Delta\overline{M}\left(\theta_n(L)+\Delta\theta(L)\right)-M_n(0)\Delta\theta(0)-\Delta M(0)\left(\theta_n(0)+\Delta\theta(0)\right).\end{aligned}\tag{13}$$

It can be easily shown that the Euler–Lagrange equations of $\Delta\Pi_{HR}$, i.e., the conditions for which $\delta\left(\Delta\Pi_{HR}\right)=0$ holds, are

$$M_n'+\Delta M'+(\overline{P}_{x_n}+\Delta\overline{P}_x)(\sin(\theta_n)+\cos(\theta_n)\Delta\theta)+(\overline{P}_{y_n}+\Delta\overline{P}_y)(\cos(\theta_n)-\sin(\theta_n)\Delta\theta)=0,\tag{14.1}$$

$$\frac{M_n}{EI}+\frac{\Delta M}{EI}-\theta_n'-\Delta\theta'=0\tag{14.2}$$

and

$$M_n(L)-\overline{M}_n+\Delta M(L)-\Delta\overline{M}=0,\tag{15.1}$$

$$\theta_n(0)+\Delta\theta(0)=0.\tag{15.2}$$

Indeed, they represent the incremental form of the boundary-value problem given by (1) and (2). Note that the incremental complementary Hellinger–Reissner functional is complete in that it makes no assumptions on moment equilibrium or compatibility in the reference state S_n. Different functionals can be developed in a similar fashion by assuming that different conditions are satisfied in the reference state.

Integrating by parts the terms containing derivatives of the rotations, and using the incremental equilibrium equations (14.1) and (15.1), gives rise to the incremental complementary energy functional, $\Delta\Pi_c:\mathcal{H}^1\to\mathcal{R}$,

$$\begin{aligned}\Delta\Pi_c(\Delta M)=\int_0^L\Bigg(&\frac{1}{2}\frac{\Delta M^2}{EI}+\frac{M_n\Delta M}{EI}+\theta_n\Delta M'\\&+\frac{1}{2}\frac{\left(M_n'+\Delta M'+(\overline{P}_{x_n}+\Delta\overline{P}_x)\sin(\theta_n)+(\overline{P}_{y_n}+\Delta\overline{P}_y)\cos(\theta_n)\right)^2}{(\overline{P}_{y_n}+\Delta\overline{P}_y)\sin(\theta_n)-(\overline{P}_{x_n}+\Delta\overline{P}_x)\cos(\theta_n)}\Bigg)\,dx.\end{aligned}\tag{16}$$

As can be seen, this functional is only expressed in terms of incremental moments. Therefore, it can be regarded as a pure incremental form of the total complementary energy (8). We note that the structure of this incremental energy functional resembles that of the total complementary energy functional introduced in [38].

The stationarity of the incremental complementary energy provides the kinematic equations. Hence, as long as the incremental equilibrium conditions are satisfied a priori, a stationary point of $\Delta\Pi_c$ corresponds to a solution to the incremental form of the boundary-value problem.

It can be easily seen that, as expected, when both $\overline{P}_x$ and $\overline{P}_y$ are zero, the last integral term in (16) becomes zero and, therefore, the problem becomes linear. As a result, the pure incremental complementary energy must be reformulated in that case and expressed as

$$\Delta\Pi_c(\Delta M)=\int_0^L\left(\frac{1}{2}\frac{\Delta M^2}{EI}+\frac{M_n\Delta M}{EI}+\theta_n\Delta M'\right)\mathrm{d}x.\tag{17}$$

This functional can be obtained in the same fashion as that of given in (16), with the incremental equilibrium equations (14.1) and (15.1) being simplified to

$$M_n'+\Delta M'=0,\tag{18.1}$$

$$M_n(L)-\overline{M}_n+\Delta M(L)-\Delta\overline{M}=0.\tag{18.2}$$

Note also that, unlike the total complementary variational principle presented in the preceding section, which corresponds, in general, to a saddle-point principle, the proposed incremental complementary variational

principle corresponds to a maximum or a minimum principle, depending on the sign of the denominator of the last term in (16). Physically, the denominator of the last term in (16) represents the axial force on the beam. This being said, the sign of the second variation of the total complementary energy depends only on the sign of the axial force applied along the beam. Indeed, if the axial force is positive, then the principle corresponds to a maximum principle.

As it only involves the bending moment field as fundamental unknown variables, this incremental principle is well suited for the development of a force-based updated Lagrangian finite element model.

It is also worth mentioning that the complementary energy-based functionals presented above include lower-order derivatives than their corresponding potential energy functionals. Hence, from a numerical point of view, the complementary variational formulations require lower-order continuity approximations than the standard displacement-based variational formulations. This is of utmost importance, since the lower the order of continuity we require for the approximation functions, the larger the range of functions we can choose from.

An advantage of the present pure incremental complementary variational approach over the total Hellinger–Reissner (mixed) variational approach developed in [39] is related to numerical stability. Indeed, the numerical discretization of a mixed variational principle is very often trickier, as it may lead to formulations with inherent numerical stability issues. In fact, certain choices of the individual approximation functions lead to mixed formulations characterized by indefinite algebraic systems that cannot be used, in general, to provide reliable numerical results [7]. On the contrary, numerical formulations relying on pure (one-field) variational approaches are unconditionally stable. The proposed finite element formulation herein developed naturally belongs to this category.

Before proceeding to the development of the finite element model, it should be emphasized that, although this functional requires the incremental form of the equilibrium equations to be satisfied a priori, there is no guarantee that equilibrium will be satisfied in the $(n+1)$-th state. This stems from the fact that the equilibrium equations are nonlinear. As a result, approximate solutions may drift away from the true solution during the incremental process, even with small increments. To avoid this, an equilibrium check might be appropriate. This may be easily accomplished by resorting to an incremental/iterative solution technique, such as a Newton–Raphson-type scheme [12]. This technique leads to more accurate solutions, regardless of the increment size, and is more efficient as fewer solution steps are required. As for the incremental kinematic equations (14.2) and (15.2), they are only enforced in a weak sense within an increment. However, as their total forms consist of linear equations, no compatibility check is required for convergence purposes.

5 Force-based updated Lagrangian finite element model

As noted above, only the incremental bending moment field needs to be approximated. Let us consider the case of piecewise-linear C^0-continuous polynomial functions, defined at the element level as

$$\Delta M_e^h = \Delta M_e^0 \frac{L_e - x_e}{L_e} + \Delta M_e^1 \frac{x_e}{L_e} \tag{19}$$

with $e = 1, 2, \ldots, n_{\text{el}}$, where n_{el} is the number of elements. ΔM_e^0 and ΔM_e^1 represent the incremental nodal bending moments defined at $x_e = 0$ and $x_e = L_e$, respectively, with L_e the length of the elements. Local coordinates to the element x_e are used.

The discretized form of the incremental complementary energy (16) can be expressed as a sum of element contributions as

$$\Delta \Pi_c^h = \sum_{e=1}^{n_{\text{el}}} \Delta \Pi_{c_e}^h \tag{20}$$

with $\Delta \Pi_{c_e}^h$ representing the incremental complementary energy associated with element e.

After placing (19) into (16), and considering a single finite element, differentiation of $\Delta \Pi_c^h$ with respect to the incremental nodal bending moments ΔM_e^0 and ΔM_e^1 gives the following algebraic linear (Euler–Lagrange) system of equations:

$$\frac{\Delta M_e^0 L_e}{3EI} + \frac{\Delta M_e^1 L_e}{6EI} + \frac{M_{n_e} L_e}{2EI} - \theta_{n_e} + \frac{\left(\Delta M_e^1 - \Delta M_e^0 + L_e(\overline{P}_{x_n} + \Delta\overline{P}_x)\sin(\theta_{n_e}) + L_e(\overline{P}_{y_n} + \Delta\overline{P}_y)\cos(\theta_{n_e})\right)}{L_e(\overline{P}_{x_n} + \Delta\overline{P}_x)\cos(\theta_{n_e}) - L_e(\overline{P}_{y_n} + \Delta\overline{P}_y)\sin(\theta_{n_e})} = 0, \tag{21.1}$$

$$\frac{\Delta M_e^0 L_e}{6EI} + \frac{\Delta M_e^1 L_e}{3EI} + \frac{M_{n_e} L_e}{2EI} + \theta_{n_e} - \frac{\left(\Delta M_e^1 - \Delta M_e^0 + L_e(\overline{P}_{x_n} + \Delta\overline{P}_x)\sin(\theta_{n_e}) + L_e(\overline{P}_{y_n} + \Delta\overline{P}_y)\cos(\theta_{n_e})\right)}{L_e(\overline{P}_{x_n} + \Delta\overline{P}_x)\cos(\theta_{n_e}) - L_e(\overline{P}_{y_n} + \Delta\overline{P}_y)\sin(\theta_{n_e})} = 0. \tag{21.2}$$

This system of equations can be recast in matrix form as

$$\boldsymbol{F}_e \Delta \boldsymbol{M}_e + \boldsymbol{\theta}_e = \boldsymbol{0} \tag{22}$$

where $\boldsymbol{F}_e$ is the element flexibility matrix given as

$$\boldsymbol{F}_e = \boldsymbol{F}_{\mathrm{MAT}_e} + \boldsymbol{F}_{\mathrm{GEO}_e}$$

with $\boldsymbol{F}_{\mathrm{MAT}_e}$ and $\boldsymbol{F}_{\mathrm{GEO}_e}$ the material and geometric flexibility matrices, respectively, given by

$$\boldsymbol{F}_{\mathrm{MAT}_e} = \frac{L_e}{EI}\begin{bmatrix} \frac{1}{3} & \frac{1}{6} \\ \frac{1}{6} & \frac{1}{3} \end{bmatrix} \quad \text{and} \quad \boldsymbol{F}_{\mathrm{GEO}_e} = -\frac{1}{L_e(\overline{P}_{x_n} + \Delta\overline{P}_x)\cos(\theta_{n_e}) - L_e(\overline{P}_{y_n} + \Delta\overline{P}_y)\sin(\theta_{n_e})}\begin{bmatrix} 1 & -1 \\ -1 & 1 \end{bmatrix}. \tag{23}$$

$\Delta \boldsymbol{M}_e$ represents the element vector of incremental nodal bending moments, whereas $\boldsymbol{\theta}_e$ represents the element vector of equivalent nodal rotations defined as the independent terms in Eqs. (21), being given as

$$\Delta \boldsymbol{M}_e = \begin{bmatrix} \Delta M_e^0 \\ \Delta M_e^1 \end{bmatrix} \quad \text{and} \quad \boldsymbol{\theta}_e = \begin{bmatrix} \frac{M_{n_e} L_e}{2EI} - \theta_{n_e} + \frac{\left(L_e(\overline{P}_{x_n}+\Delta\overline{P}_x)\sin(\theta_{n_e})+L_e(\overline{P}_{y_n}+\Delta\overline{P}_y)\cos(\theta_{n_e})\right)}{L_e(\overline{P}_{x_n}+\Delta\overline{P}_x)\cos(\theta_{n_e})-L_e(\overline{P}_{y_n}+\Delta\overline{P}_y)\sin(\theta_{n_e})} \\ \frac{M_{n_e} L_e}{2EI} + \theta_{n_e} - \frac{\left(L_e(\overline{P}_{x_n}+\Delta\overline{P}_x)\sin(\theta_{n_e})+L_e(\overline{P}_{y_n}+\Delta\overline{P}_y)\cos(\theta_{n_e})\right)}{L_e(\overline{P}_{x_n}+\Delta\overline{P}_x)\cos(\theta_{n_e})-L_e(\overline{P}_{y_n}+\Delta\overline{P}_y)\sin(\theta_{n_e})} \end{bmatrix}. \tag{24}$$

After performing simple direct allocation operations on the elementary systems of equations, the assembled (global) governing system of algebraic equations for the finite element mesh is obtained as

$$\boldsymbol{F} \Delta \boldsymbol{M} = \boldsymbol{\theta} \tag{25}$$

with $\boldsymbol{F}$ the assembled flexibility matrix, and $\Delta \boldsymbol{M}$ and $\boldsymbol{\theta}$ the assembled vectors of incremental nodal bending moments and equivalent nodal rotations, respectively, defined as

$$\boldsymbol{\Delta M} = \begin{bmatrix} \Delta M_0 \\ \Delta M_1 \\ \vdots \\ \Delta M_{n_{el}} \end{bmatrix} \quad \text{and} \quad \boldsymbol{\theta} = \begin{bmatrix} \theta_0 \\ \theta_1 \\ \vdots \\ \theta_{n_{el}} \end{bmatrix} \tag{26}$$

where ΔM_i, $i = 0, 1, 2, \ldots, n_{\mathrm{el}}$ represent the global incremental nodal bending moments, and θ_j, $j = 0, 1, 2, \ldots, n_{\mathrm{el}}$, represent the equivalent nodal rotations. The adopted assembly procedure is similar to the standard one employed for displacement-based models, see e.g., [21].

Note that the proposed finite element model makes use of C^0-continuous approximate bending moments, with the nodal moments as the fundamental unknowns. Hence, moment continuity along the interelement boundaries is automatic. This resembles indeed the traditional displacement-based Galerkin finite element model with nodal displacement unknowns. As a result, the present formulation avoids the need to resort to Lagrange multipliers to enforce interelement moment equilibrium, a procedure usually leading to (computationally more demanding and conditionally stable) hybrid finite element formulations.

Being an incremental approach, the total load is divided into increments. In each load increment, the incremental complementary energy is defined from the last known solution and minimized/maximized to

obtain the next solution increment. Since there is no guarantee that equilibrium will be satisfied in the $(n+1)$-th state, an iterative procedure based on the Newton–Raphson algorithm is then activated to correct the solution, avoiding the so-called drift-off errors during the incremental process. This solution is used as an initial state, and the load is incremented upward. This process is continued until the desired load level is reached.

The Newton–Raphson iterative algorithm is driven by the equilibrium differential equation (1.1). This amounts to setting the residue at the (i)-th iteration as

$$R^{(i)} := EIM'^{(i)}_{n+1} + \overline{P}_{x_{n+1}} \sin(\theta^{(i)}_{n+1}) + \overline{P}_{y_{n+1}} \cos(\theta^{(i)}_{n+1}). \tag{27}$$

The iterations are repeated until the following convergence criterion is satisfied:

$$|R^{(i)}| \leq tol \tag{28}$$

where tol is a sufficiently small specified equilibrium absolute convergence tolerance. The corresponding bending moment $M^{(i)}_{n+1}$ is then accepted as sufficiently close to the solution of the discrete boundary-value problem and used afterward to compute $\theta^{(i)}_{n+1}$ from Eq. (14.1).

The displacements u^h and w^h can be computed in the end of the iterative process by integrating Eqs. (3.1) and (3.2), respectively, along the elements. The constants of integration that arise can be uniquely determined by enforcing the continuity conditions and boundary kinematic conditions (3.3), thus leading to a globally C^0-continuous displacement field (u^h, w^h).

6 Numerical examples

To validate and assess the accuracy of the proposed force-based finite element model (referred hereafter to as the FB-model), some examples were solved and their solutions compared with those obtained using a standard displacement-based two-node finite element model with piecewise C^0-continuous rotations (referred hereafter to as the DB-model). Note that, for a given mesh, both models employ the same number of degrees of freedom, thus leading to numerical simulations with similar computational costs.

Numerical solutions computed using the FB-model are hereafter denoted with a subscript index c, whereas those computed using the DB-model are hereafter denoted with a subscript index p.

All reference solutions were computed using the DB-model with uniform meshes of 256 elements.

An exact analytical integration scheme was used in both FB- and DB-models.

A consistent system of units has been used for all physical quantities that define the selected numerical examples.

For all computations, the bending stiffness was set to $EI = 1$, and the length of the cantilever was set to $L = 1$.

Finite element meshes of 2, 4, 8, 16 and 32 elements were adopted in all examples. However, only the solutions computed using 2, 4, 8 and 16 elements were included in the plots. As for the tabular results, all solutions corresponding to the five meshes were presented. Throughout the various examples, the plots in red, green, blue and orange correspond to the approximate solutions obtained using 2, 4, 8 and 16 elements, respectively.

6.1 Load case 1: $\overline{P}_x = 0,\ \overline{P}_y = 0,\ \overline{M} = 2\pi$

The classical problem of a cantilever subject to a bending moment at the free end is first studied. The applied bending moment was set to $\overline{M} = 2\pi$. In this particular case, the problem is linear and the exact analytical solution is known. The exact deformed shape of the cantilever is a perfect circle, and the bending curvature and bending moment fields are constant along the cantilever, see e.g., [39]. The analyses were carried out in 10 load steps. Due to the linearity of the problem, no Newton–Raphson iterations were required.

The obtained equilibrium paths representing the evolution of the tip rotations with respect to the load steps are depicted in Fig. 2.

The computed deflections of the cantilever are depicted in Fig. 3. We note that, contrarily to the DB-model, the FB-model does not enforce compatibility in strong form. As a result, not only the approximate rotation fields are discontinuous across interelement boundaries, but also the kinematic condition $\theta(0) = 0$ is violated.

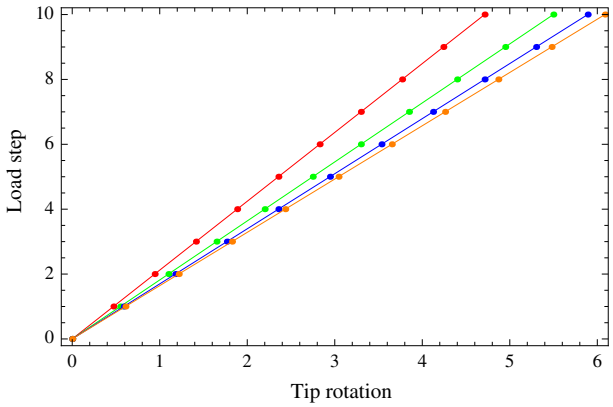

Fig. 2 Tip rotation versus load step for $\overline{P}_x = 0$, $\overline{P}_y = 0$, $\overline{M} = 2\pi$. 2, 4, 8 and 16 finite element mesh solutions depicted in *red*, *green*, *blue*, and *orange*, respectively (color figure online)

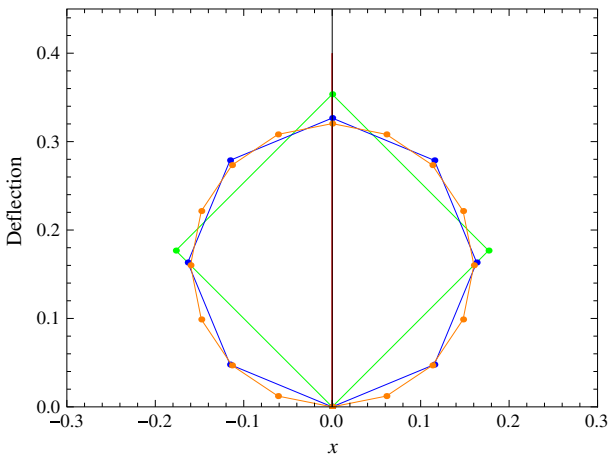

Fig. 3 Deflection of the cantilever for $\overline{P}_x = 0$, $\overline{P}_y = 0$, $\overline{M} = 2\pi$. 2, 4, 8 and 16 finite element mesh solutions depicted in *red*, *green*, *blue*, and *orange*, respectively (color figure online)

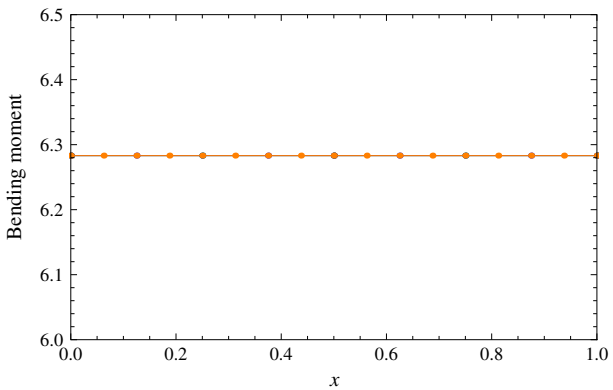

Fig. 4 Bending moments of the cantilever for $\overline{P}_x = 0$, $\overline{P}_y = 0$, $\overline{M} = 2\pi$. 2, 4, 8 and 16 finite element mesh solutions depicted in *red*, *green*, *blue*, and *orange*, respectively (color figure online)

However, this lack of compatibility decreases as the number of finite elements increases, tending to zero in the limit as the number of elements tends to infinity.

The obtained distributions of bending moments are depicted in Fig. 4. As it can be seen, all distributions are coincident to one another and match the exact solution. In other words, both the FB and DB finite element models are capable of producing the exact solution, given by $M = 2\pi$ in this case.

Table 1 Tip rotation for $\overline{P}_x = 0,\ \overline{P}_y = 0,\ \overline{M} = 2\pi$; reference solution is $\theta_{\text{ref}} = 6.28319$

n_{el}	2	4	8	16	32
$\theta_{\text{c}}^h(L)$	4.71239	5.49779	5.89048	6.08683	6.18501
$\theta_{\text{p}}^h(L)$	6.28319	6.28319	6.28319	6.28319	6.28319

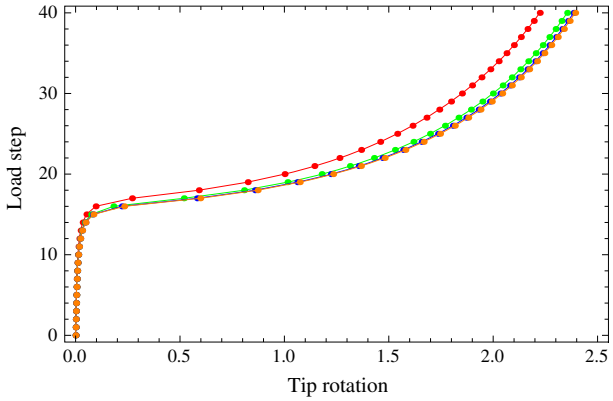

Fig. 5 Tip rotation versus load step for $\overline{P}_x = 6,\ \overline{P}_y = 0.04,\ \overline{M} = 0.\ 2,\ 4,\ 8$ and 16 finite element mesh solutions depicted in *red*, *green*, *blue*, and *orange*, respectively (color figure online)

The obtained tip rotations are indicated in Table 1. As expected, only the DB-model is capable of capturing the exact solution in this case, as it is based on piecewise-linear continuous rotations, contrarily to the FB-model, which gives piecewise-constant discontinuous rotations.

The obtained total potential and total complementary energies of the DB- and FB-solutions all match the exact one, given by $\Pi_c = -\Pi_p = 19.73921$ in this case. This confirms the capability of both the DB- and FB-models to produce the exact solution in this specific problem.

6.2 Load case 2: $\overline{P}_x = 6,\ \overline{P}_y = 0.04,\ \overline{M} = 0$

The cantilever is now assumed to be subject to $\overline{P}_x = 6$ and $\overline{P}_y = 0.04$. We are particularly interested in studying the post-buckling behavior of the cantilever. The small vertical load $\overline{P}_y$ was introduced to artificially induce buckling instability of the cantilever. The analyses were carried out in 40 load steps. The absolute convergence tolerance for the Newton–Raphson method was set to 10^{-9}.

The obtained equilibrium paths are depicted in Fig. 5. As it can be observed, except for the mesh only with 2 elements, all the other meshes render solutions relatively close to one another.

The deflections of the cantilever are depicted in Fig. 6. Clearly, the cantilever is under truly large displacements and rotations for the adopted applied load values.

The distributions of bending moments are depicted in Fig. 7. As expected, all distributions are continuous along the interelement boundaries and satisfy the equilibrium boundary condition given by $M(L) = 0$. The numerical values of the bending moments computed using the FB- and DB-models at $x = 0$ are indicated in Table 2 along with the reference solution. As it can be seen, for a given discretization, the FB-model gives bending moments that are more accurate than those produced by the DB-model. Further, we can see from Table 2 that, while the DB-bending moments converge from below to the exact solution, the FB-bending moments converge from above to the exact solution.

The computed tip rotations are indicated in Table 3. As expected, unlike the case of the bending moments, the computed tip rotations obtained with the DB-model are more accurate than those rendered by the FB-model. Further, analyzing Table 3, we observe that the convergence of the tip rotations to the exact solution is reversed with respect to that of the bending moments defined at $x = L$.

The total potential and total complementary energies associated with the FB- and DB-solutions are displayed in Table 4. Analyzing Table 4, it can be observed that although for the two first meshes the errors of the FB-solution with respect to the reference solution are smaller than those of the DB-solution, for the remaining

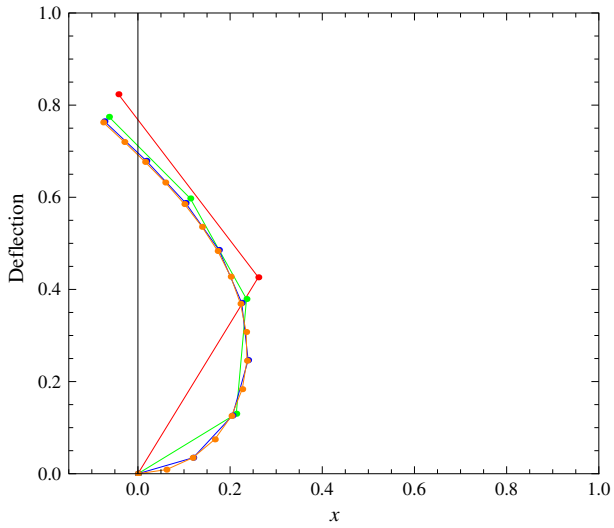

Fig. 6 Deflection of the cantilever for $\overline{P}_x = 6$, $\overline{P}_y = 0.04$, $\overline{M} = 0.\ 2, 4, 8$ and 16 finite element mesh solutions depicted in *red*, *green*, *blue*, and *orange*, respectively (color figure online)

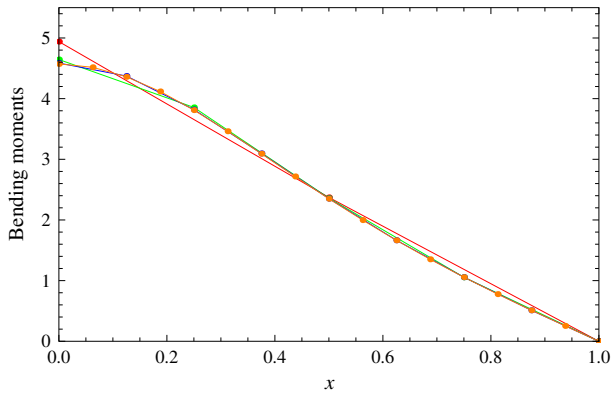

Fig. 7 Bending moments of the cantilever for $\overline{P}_x = 6$, $\overline{P}_y = 0.04$, $\overline{M} = 0.\ 2, 4, 8$ and 16 finite element mesh solutions depicted in *red*, *green*, *blue*, and *orange*, respectively (color figure online)

Table 2 Bending moment at support for $\overline{P}_x = 6$, $\overline{P}_y = 0.04$, $\overline{M} = 0$; reference solution is $M_{\text{ref}} = 4.56784$

n_{el}	2	4	8	16	32
$M_{\text{c}}^h(0)$	4.94002	4.64488	4.58643	4.57245	4.56898
$M_{\text{p}}^h(0)$	3.74611	4.30949	4.49669	4.54903	4.56279

Table 3 Tip rotation for $\overline{P}_x = 6$, $\overline{P}_y = 0.04$, $\overline{M} = 0$; reference solution is $\theta_{\text{ref}} = 2.39533$

n_{el}	2	4	8	16	32
$\theta_{\text{c}}^h(L)$	2.22322	2.35439	2.38536	2.39285	2.39471
$\theta_{\text{p}}^h(L)$	2.44579	2.40846	2.39860	2.39615	2.39553

discretizations the errors of the DB- and FB-solutions are almost identical. It is also worth mentioning that both the total complementary and the total potential energies converge from below to the reference solution.

The convergence of the errors of the solutions measured in total energy as the difference between the obtained energies and the reference one is shown in Fig. 8. As it can be seen, the convergence rates of the FB- and DB-models are identical.

Table 4 Total energies for $\overline{P}_x = 6,\ \overline{P}_y = 0.04,\ \overline{M} = 0$; reference solution is $\Pi_{ref} = 2.54136$

n_{el}	2	4	8	16	32
Π_c^h	2.33918	2.48401	2.52687	2.53776	2.54050
$-\Pi_p^h$	2.30784	2.48304	2.52672	2.53773	2.54049

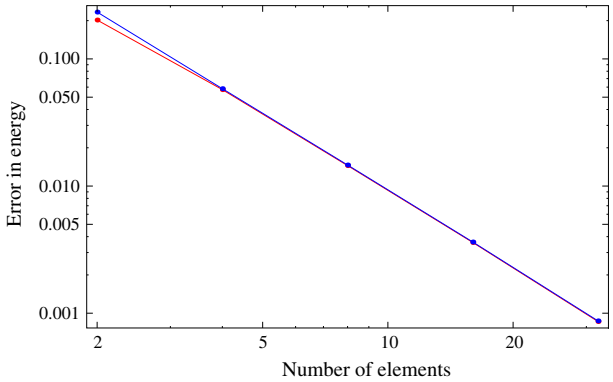

Fig. 8 Convergence of the errors in energy with respect to the number of elements for $\overline{P}_x = 6,\ \overline{P}_y = 0.04$. FB-solution errors in *red*; DB-solution errors in *blue* (color figure online)

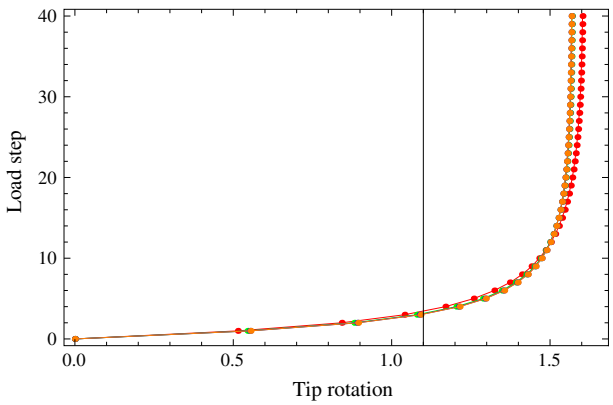

Fig. 9 Tip rotation versus load step for $\overline{P}_x = 0,\ \overline{P}_y = 50,\ \overline{M} = 0$. 2, 4, 8 and 16 finite element mesh solutions depicted in *red*, *green*, *blue*, and *orange*, respectively (color figure online)

6.3 Load case 3: $\overline{P}_x = 0,\ \overline{P}_y = 50,\ \overline{M} = 0$

In this problem, the cantilever is assumed to be subject only to $\overline{P}_y = 50$. The analyses were carried out in 40 load steps. The absolute convergence tolerance for the Newton–Raphson method was set to 10^{-9}.

The obtained equilibrium paths depicting the tip rotation versus the load step are presented in Fig. 9. Given the large value adopted for the vertical load, the equilibrium paths exhibit a vertical asymptote for a rotation angle close to $\pi/2$.

The obtained deflections of the cantilever are depicted in Fig. 10.

The distributions of bending moments are depicted in Fig. 11. As in the preceding problem, all distributions are continuous along the interelement boundaries and satisfy the equilibrium boundary condition given by $M(L) = 0$. The numerical values of the bending moments at $x = 0$ computed using the FB- and DB-models are indicated in Table 5 along with the reference solution. Once again, the FB-model proves to be more accurate than the DB-model in predicting bending moment distributions.

The obtained tip rotations are indicated in Table 6. Indeed, although the DB-tip rotations come out as more accurate than those rendered by the FB-model, the relative errors of the computed FB-rotations with respect to the reference solution are smaller than those of the bending moments provided by the DB-model. This seems to indicate that the FB-model is more accurate in overall than the DB-model.

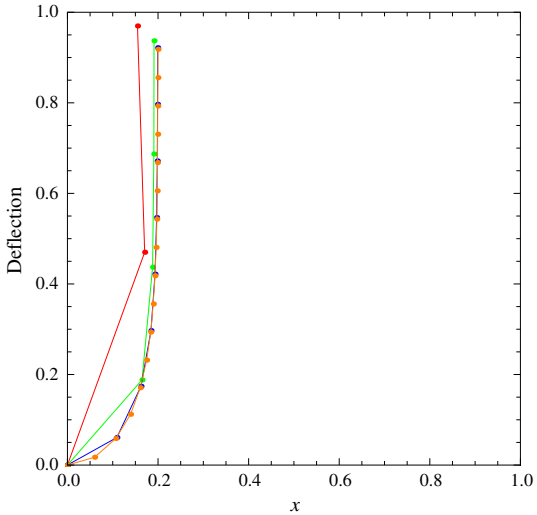

Fig. 10 Deflection of the cantilever for $\overline{P}_x = 0$, $\overline{P}_y = 50$, $\overline{M} = 0$. 2, 4, 8 and 16 finite element mesh solutions depicted in *red*, *green*, *blue*, and *orange*, respectively (color figure online)

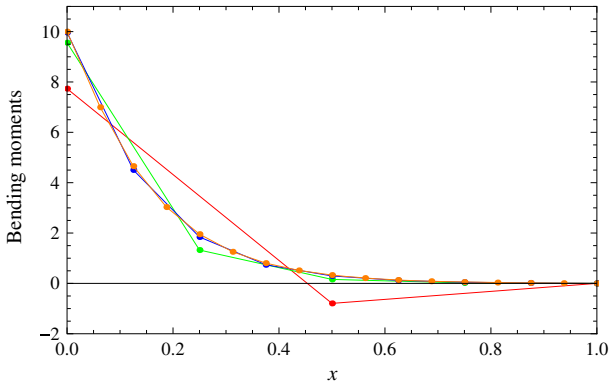

Fig. 11 Bending moments of the cantilever for $\overline{P}_x = 0$, $\overline{P}_y = 50$, $\overline{M} = 0$. 2, 4, 8 and 16 finite element mesh solutions depicted in *red*, *green*, *blue*, and *orange*, respectively (color figure online)

Table 5 Bending moment at support for $\overline{P}_x = 0$, $\overline{P}_y = 50$, $\overline{M} = 0$; reference solution is $M_{\text{ref}} = 9.99998$

n_{el}	2	4	8	16	32
$M_{\text{c}}^h(0)$	7.73327	9.55828	9.96396	9.99780	9.99985
$M_{\text{p}}^h(0)$	3.41476	5.40669	7.25452	8.51518	9.23432

Table 6 Tip rotation for $\overline{P}_x = 0$, $\overline{P}_y = 50$, $\overline{M} = 0$; reference solution is $\theta_{\text{ref}} = 1.56798$

n_{el}	2	4	8	16	32
$\theta_{\text{c}}^h(L)$	1.60255	1.56931	1.56824	1.56804	1.56780
$\theta_{\text{p}}^h(L)$	1.54219	1.57006	1.56858	1.56814	1.56802

The total potential and total complementary energies associated with the FB- and DB-solutions are presented in Table 7. It can be seen that the total potential and total complementary energies converge from below and from above, respectively, to the reference solution. This result indicates convexity/concavity of the total potential/complementary energies at the computed solution and may be used to compute global upper bounds of the error of the approximate solutions.

The convergence results are shown in Fig. 12. As in the previous load case, the convergence rates of the FB- and DB-models are identical.

Table 7 Total energies for $\overline{P}_x = 0,\ \overline{P}_y = 50,\ \overline{M} = 0$; reference solution is $\Pi_{ref} = 41.71586$

n_{el}	2	4	8	16	32
Π_c^h	43.91113	42.35838	41.85759	41.74853	41.72375
$-\Pi_p^h$	38.62877	40.89322	41.51398	41.66592	41.70333

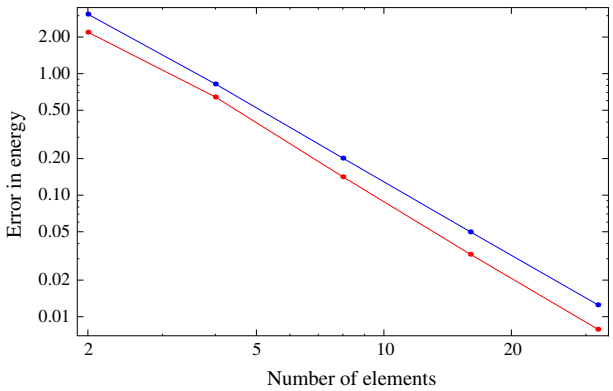

Fig. 12 Convergence of the errors in energy with respect to the number of elements for $\overline{P}_x = 0,\ \overline{P}_y = 50,\ \overline{M} = 0$. FB-solution errors in *red*; DB-solution errors in *blue* (color figure online)

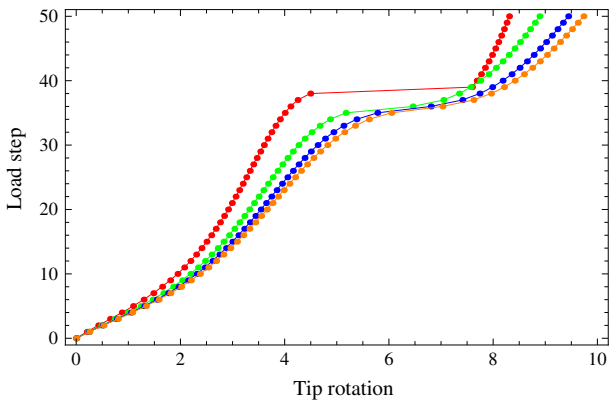

Fig. 13 Tip rotation versus load step for $\overline{P}_x = 6,\ \overline{P}_y = 5,\ \overline{M} = 10$. 2, 4, 8 and 16 finite element mesh solutions depicted in *red*, *green*, *blue*, and *orange*, respectively (color figure online)

6.4 Load case 4: $\overline{P}_x = 6,\ \overline{P}_y = 5,\ \overline{M} = 10$

The cantilever is now assumed to be subject to $\overline{P}_x = 6,\ \overline{P}_y = 5$ and $\overline{M} = 10$. The analyses were carried out in 50 load steps. The absolute convergence tolerance for the Newton–Raphson method was set to 10^{-9}.

The obtained equilibrium paths are depicted in Fig. 13. The relative distances between all these paths show that the present problem exhibits a highly nonlinear behavior.

The computed deflections of the cantilever are plotted in Fig. 14. We observe that the mesh only with 2 elements is too coarse to give an approximate solution close enough to the exact one. A more detailed view of the deflection shapes of the cantilever with 4, 8 and 16 element meshes can be seen in Fig. 15.

The distributions of bending moments are depicted in Fig. 16. As before, all distributions are statically admissible. This is of utmost importance in engineering design, as it avoids the need for the so-called averaging procedures required when using the traditional DB-model, as it produces discontinuous bending moment distributions. The numerical values of the bending moments computed using the FB- and DB-models at $x = 0$ are indicated in Table 8 and compared to the reference solution. Similarly to all previous numerical examples, for a given discretization, the FB-model renders more accurate bending moments than those produced by the DB-model.

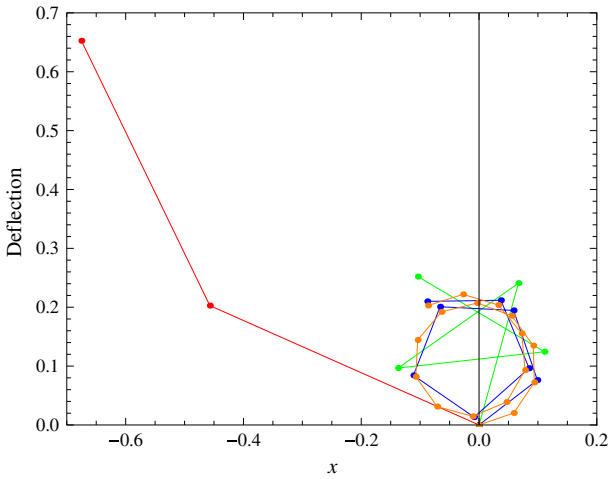

Fig. 14 Deflection of the cantilever for $\overline{P}_x = 6$, $\overline{P}_y = 5$, $\overline{M} = 10$—global view. 2, 4, 8 and 16 finite element mesh solutions depicted in *red*, *green*, *blue*, and *orange*, respectively (color figure online)

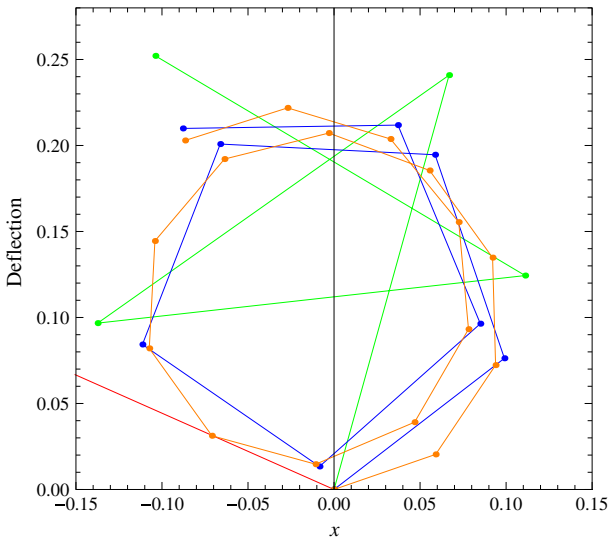

Fig. 15 Deflection of the cantilever for $\overline{P}_x = 6$, $\overline{P}_y = 5$, $\overline{M} = 10$—view of the three last solutions. 2, 4, 8 and 16 finite element mesh solutions depicted in *red*, *green*, *blue*, and *orange*, respectively (color figure online)

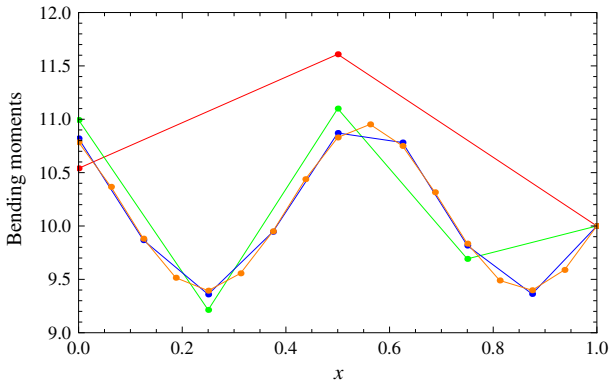

Fig. 16 Bending moments of the cantilever for $\overline{P}_x = 6$, $\overline{P}_y = 5$, $\overline{M} = 10$. 2, 4, 8 and 16 finite element mesh solutions depicted in *red*, *green*, *blue*, and *orange*, respectively (color figure online)

Table 8 Bending moment at support for $\overline{P}_x = 6,\ \overline{P}_y = 5,\ \overline{M} = 10$; reference solution is $M_{\text{ref}} = 10.77342$

n_{el}	2	4	8	16	32
$M^h_{\text{c}}(0)$	10.54008	10.99356	10.82025	10.78476	10.77620
$M^h_{\text{p}}(0)$	9.99007	9.93803	10.35181	10.58196	10.68551

Table 9 Tip rotation for $\overline{P}_x = 6,\ \overline{P}_y = 5,\ \overline{M} = 10$; reference solution is $\theta_{\text{ref}} = 10.03755$

n_{el}	2	4	8	16	32
$\theta^h_{\text{c}}(L)$	8.30540	8.88851	9.44027	9.73270	9.88328
$\theta^h_{\text{p}}(L)$	10.05688	10.02607	10.03648	10.03729	10.03747

Table 10 Total energies for $\overline{P}_x = 6,\ \overline{P}_y = 5,\ \overline{M} = 10$; reference solution is $\Pi_{ref} = 57.38625$

n_{el}	2	4	8	16	32
Π^h_c	62.78616	57.76473	57.45632	57.40255	57.39021
$-\Pi^h_p$	57.25106	57.31614	57.36691	57.38120	57.38493

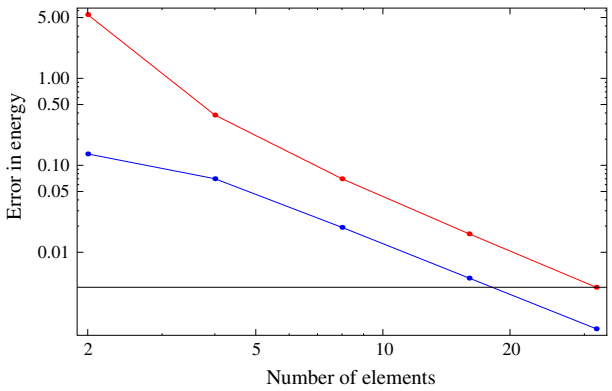

Fig. 17 Convergence of the errors in energy with respect to the number of elements for $\overline{P}_x = 6,\ \overline{P}_y = 5,\ \overline{M} = 10$. FB-solution errors in *red*; DB-solution errors in *blue* (color figure online)

The obtained tip rotations are indicated in Table 9. As in the previous load case, the DB-tip rotations come out as more accurate than those rendered by the FB-model.

The convergence of the total potential and total complementary energies associated with the FB- and DB-solutions is presented in Table 10. As in the preceding problem, the total potential and total complementary energies converge from below and from above, respectively, to the reference solution.

The convergence results are shown in Fig. 17. As in the previous load cases, the convergence rates of the FB- and DB-models are similar.

7 Conclusions

We have introduced a variationally consistent force-based updated Lagrangian finite element formulation for the geometrically nonlinear analysis of beams modeled by the Euler–Bernoulli version of the elastica theory. This formulation relies on a pure incremental complementary energy principle only expressed in terms of bending moment fields. Based on this formulation, a new two-node, rotation-free, finite beam element has been developed for the analysis of problems with arbitrarily large displacements and rotations. The proposed model resembles the standard C^0-continuous Lagrange (or two-node) displacement-based model with piecewise-linear rotations. To assess the accuracy of the proposed model, we have analyzed a cantilever beam problem with different loading conditions. The numerical results show that the proposed FB-model produces more accurate bending moment distributions than those rendered by the traditional two-node DB-model. In particular, the obtained bending moments satisfy the equilibrium differential equation in strong form and are continuous across

the interelement boundaries. The obtained numerical results also demonstrate that, for a given problem, both the proposed FB- and DB-models are characterized by the same convergence rate. Further, it was numerically shown that, in some cases, pairing the computed total potential and total complementary energies of the DB- and FB-numerical solutions, respectively, allows to determine global upper bounds of the error of the approximate solutions with respect to the exact solution. This is of utmost importance in engineering design. The formulation can be extended to beams with other boundary conditions and/or loading conditions, as well as to initially curved beams. The formulation can also be generalized to the case of planar framed structures.

References

1. Antman, S.S.: Nonlinear Problems of Elasticity, 2nd edn. Springer, New York (1995)
2. Atanackovic, T.M., Spasic, D.T.: A model for plane elastica with simple shear deformation pattern. Acta Mech. **104**, 241–253 (1994)
3. Backlund, J.: Large deflection analysis of elasto-plastic beams and frames. Int. J. Mech. Sci. **18**, 269–277 (1976)
4. Bathe, K.J.: Finite Element Procedures. Prentice-Hall, New Jersey (1996)
5. Bathe, K.J., Bolourchi, S.: Large displacement analysis of three-dimensional beam structures. Int. J. Numer. Methods Eng. **14**, 961–986 (1979)
6. Bisshopp, K.E., Drucker, D.C.: Large deflections of cantilever beams. Q. Appl. Math. **3**, 272–275 (1945)
7. Brezzi, F., Fortin, M.: Mixed and Hybrid Finite Element Methods, 15th edn. Springer Series in Computational Mathematics. Springer, London (1991)
8. Campanile, L.F., Hasse, A.: A simple and effective solution to the elastica problem. J. Mech. Eng. Sci. **222**, 2513–2516 (2008)
9. Carol, I., Murcia, J.: Nonlinear time-dependent analysis of planar frames using an 'exact' formulation—I: theory. Comput. Struct. **33**, 79–87 (1989)
10. Chan, T.F., Kang, S.H., Shen, J.: Euler's elastica and curvature-based inpainting. SIAM J. Appl. Math. **63**, 564–592 (2002)
11. Chen, L.: An integral approach for large deflection cantilever beams. Int. J. Non-Linear Mech. **45**, 301–305 (2010)
12. Crisfield, M.A.: Non-linear Finite Element Analysis of Solids and Structures. Volume 1: Essentials. Wiley, New York (1991)
13. de Fraeijs Veubeke, B.: Upper and lower bounds in matrix structural analysis. In: AGARDograph 72: Matrix Methods of Structural Analysis. Pergamon Press, London (1964)
14. de Fraeijs Veubeke, B.: Stress analysis. In: Displacement and Equilibrium Models in the Finite Element Method, pp. 145–197. Wiley, New York (1965)
15. Debongnie, J.F., Zhong, H.G., Beckers, P.: Dual analysis with general boundary conditions. Comput. Methods Appl. Mech. Eng. **122**, 183–192 (1995)
16. Dedè, L., Santos, H.A.F.A.: B-spline goal-oriented error estimators for geometrically nonlinear rods. Comput. Mech. **49**, 35–52 (2012)
17. Euler, L.: Methodus inveniendi lineas curvas maximi minimive proprietate gaudentes (appendix, de curvis elasticis). Lausanne und Genf, 1744 (1774)
18. Golley, B.W.: The finite element solution to a class of elastica problems. Comput. Methods Appl. Mech. Eng. **26**, 159–168 (1984)
19. Golley, B.W.: The solution of open and closed elasticas using intrinsic coordinate finite elements. Comput. Methods Appl. Mech. Eng. **146**, 127–134 (1997)
20. Goss, V.G.A.: The history of the planar elastica: insights into mechanics and scientific method. Sci. Educ. **18**, 1057–1082 (2009)
21. Hughes, T.J.R.: The Finite Element Method: Linear Static and Dynamic Finite Element Analysis. Dover, New York (2000)
22. Humer, A.: Elliptic integral solution of the extensible elastica with a variable length under a concentrated force. Acta Mech. **222**, 209–223 (2011)
23. Humer, A.: Exact solutions for the buckling and postbuckling of shear-deformable beams. Acta Mech. **224**, 1493–1525 (2013)
24. Kimia, B.B., Frankel, I., Popescu, A.-M.: Euler spiral for shape completion. Int. J. Comput. Vis. **54**, 159–182 (2003)
25. Lan, P., Shabana, A.A.: Integration of b-spline geometry and ancf finite element analysis. Nonlinear Dyn. **61**, 193–206 (2010)
26. Lee, K.: Post-buckling of uniform cantilever column under a combined load. Int. J. Non-Linear Mech. **36**, 813–816 (2001)
27. Levyakov, S.V., Kuznetsov, V.V.: Stability analysis of planar equilibrium configurations of elastic rods subjected to end loads. Acta Mech. **211**, 73–87 (2010)
28. Love, A.E.H.: A Treatise on the Mathematical Theory of Elasticity, 4th edn. Cambridge University Press, Cambridge (1906)
29. Mikata, Y.: Complete solution of elastica for a clamped-hinged beam, and its applications to a carbon nanotube. Acta Mech. **190**, 133–150 (2007)
30. Mumford, D.: Algebraic Geometry and its Applications, Elastica and Computer Vision, pp. 491–506. New York (1994)
31. Mutyalarao, M., Bharathi, D., Rao, B.N.: On the uniqueness of large deflections of a uniform cantilever beam under a tip-concentrated rotational load. Int. J. Non-Linear Mech. **45**, 433–441 (2010)
32. Nallathambi, A.K., Rao, C.L., Srinivasan, S.M.: Large deflection of constant curvature cantilever beam under follower load. Int. J. Mech. Sci. **52**, 440–445 (2010)
33. Neuenhofer, A., Filippou, F.C.: Geometrically nonlinear flexibility-based frame finite element. J. Struct. Eng. ASCE **124**, 704–711 (1998)
34. Petrolito, J., Legge, K.A.: Unified nonlinear elastic frame analysis. Comput. Struct. **60**, 21–30 (1996)
35. Petrolito, J., Legge, K.A.: Nonlinear analysis of frames with curved members. Comput. Struct. **79**, 727–735 (2001)
36. Saalschutz, L.: Der belastete Stab unter Einwirkung einer seitlichen Kraft: Auf Grundlage des strengen Ausdrucks für den Krümmungsradius. Teubner (1880)

37. Santos, H.A.F.A.: Complementary-energy methods for geometrically non-linear structural models: an overview and recent developments in the analysis of frames. Arch. Comput. Methods Eng. **18**, 405–440 (2011)
38. Santos, H.A.F.A.: Variationally consistent force-based finite element method for the geometrically non-linear analysis of Euler–Bernoulli framed structures. Finite Elem. Anal. Des. **53**, 24–36 (2012)
39. Santos, H.A.F.A., Moitinho de Almeida, J.P.: Equilibrium-based finite element formulation for the geometrically exact analysis of planar framed structures. J. Eng. Mech. **136**, 1474–1490 (2010)
40. Santos, H.A.F.A., Almeida Paulo, C.I.: On a pure complementary energy principle and a force-based finite element formulation for non-linear elastic cables. Int. J. Non-Linear Mech. **46**, 395–406 (2011)
41. Santos, H.A.F.A., Pimenta, P.M., Moitinho de Almeida, J.P.: A hybrid-mixed finite element formulation for the geometrically exact analysis of three-dimensional framed structures. Comput. Mech. **48**, 591–613 (2011)
42. Schmidt, W.F.: Finite element solutions for the elastica. J. Eng. Mech. Div. **103**, 1171–1175 (1977)
43. Sreekumar, M., Nagarajan, T., Singaperumal, M.: Design of a shape memory alloy actuated compliant smart structure: elastica approach. J. Mech. Des. **131**, 061008 (2009)
44. Tang, T., Jagota, A., Hui, C.-Y.: Adhesion between single-walled carbon nanotubes. J. Appl. Phys. **97**, 074304–074304–6 (2005)
45. Timoshenko, S.P.: History of Strength of Materials. McGraw-Hill, New York (1953)
46. van der Heijden, G.H.M., Neukirch, S., Goss, V.G.A., Thompson, J.M.T.: Instability and self-contact phenomena in the writhing of clamped rods. Int. J. Mech. Sci. **45**, 161–196 (2003)
47. Washizu, K.: Variational Methods in Elasticity and Plasticity, 3rd edn. Pergamon Press, Oxford (1982)